Earth's Future

RESEARCH ARTICLE
10.1029/2021EF002511

Future Population Exposure to Daytime and Nighttime Heat Waves in South Asia

Safi Ullah[1], Qinglong You[1,2], Deliang Chen[3], D. A. Sachindra[4], Amir AghaKouchak[5], Shichang Kang[6], Mingcai Li[7], Panmao Zhai[8], and Waheed Ullah[9]

[1]Department of Atmospheric and Oceanic Sciences and Institute of Atmospheric Sciences, Fudan University, Shanghai, China, [2]Innovation Center of Ocean and Atmosphere System, Zhuhai Fudan Innovation Research Institute, Zhuhai, China, [3]Department of Earth Sciences, Regional Climate Group, University of Gothenburg, Gothenburg, Sweden, [4]Department of Hydrology and Climatology, Faculty of Earth Sciences and Spatial Management, Maria Curie-Sklodowska University, Lublin, Poland, [5]Department of Civil and Environmental Engineering, University of California, Irvine, CA, USA, [6]State Key Laboratory of Cryospheric Sciences, Northwest Institute of Eco-Environment and Resources, Chinese Academy of Sciences, Lanzhou, China, [7]Tianjin Institute of Meteorological Science, Tianjin, China, [8]State Key Laboratory of Severe Weather, Chinese Academy of Meteorological Sciences, Beijing, China, [9]School of Geographical Sciences, Nanjing University of Information Science and Technology, Nanjing, China

Key Points:

- The number and extent of heat waves (HWs) are projected to increase under all the Shared Socioeconomic Pathways (SSPs)
- The population exposure to HWs ranges from 185 to 555 million people-event with the highest exposure in the Indo-Gigantic Plain
- Compounding effects of climate change and population increase substantially aggravate exposure to HWs

Correspondence to:

Q. You,
yqingl@126.com

Citation:

Ullah, S., You, Q., Chen, D., Sachindra, D. A., AghaKouchak, A., Kang, S., et al. (2022). Future population exposure to daytime and nighttime heat waves in South Asia. *Earth's Future*, *10*, e2021EF002511. https://doi.org/10.1029/2021EF002511

Received 21 OCT 2021
Accepted 6 APR 2022

Author Contributions:

Conceptualization: Safi Ullah, Qinglong You, Panmao Zhai
Data curation: Mingcai Li, Waheed Ullah
Formal analysis: Safi Ullah, D. A. Sachindra, Waheed Ullah
Funding acquisition: Qinglong You, Deliang Chen
Methodology: Safi Ullah, Qinglong You, Deliang Chen
Project Administration: Safi Ullah, Qinglong You, Shichang Kang, Panmao Zhai
Resources: Qinglong You
Software: Safi Ullah, D. A. Sachindra, Waheed Ullah
Supervision: Qinglong You
Validation: Safi Ullah, D. A. Sachindra, Amir AghaKouchak

Abstract Climate change is expected to result in more frequent and intense heat waves (HWs) in South Asia (SA). The simultaneous increases in temperature and population will exacerbate the population exposure to future HWs. Here we estimate the future population exposure to daytime and nighttime HWs in SA using the Coupled Model Intercomparison Project 6 (CMIP6) models under four Shared Socioeconomic Pathways (SSPs) during 2061–2100, relative to 1975–2014. The results show that the projected frequency and spatial extent of the daytime (nighttime) HWs will be higher under scenario SSP5-8.5, followed by SSP2-4.5, SSP3-7.0, and SSP1-2.6 (SSP5-8.5, followed by SSP3-7.0, SSP2-4.5, and SSP1-2.6), relative to the historical period. The approach presented here allows decomposing the effects of climate change and future population on the overall exposure. The results reveal that the compounding effects of projected trends in population and HWs will significantly escalate the population exposure to HWs. Under the selected SSPs, the total population exposure to daytime and nighttime HWs ranges from 185 to 492 and 204–555 million people-event, respectively, with the maximum exposure occurring in the Indo-Gigantic Plain. The wide range of exposed populations highlights the sensitivity of the overall exposure to our future socioeconomic pathway decisions, emphasizing the importance of curbing anthropogenic greenhouse gas emissions and adopting sustainable urban planning solutions to minimize the potential socioeconomic and health impacts of HWs.

Plain Language Summary Climate change will intensify the occurrence and intensity of heatwaves (HWs) in South Asia, with severe impacts on the population. Here we estimate the population exposure to daytime and nighttime HWs using the Coupled Model Intercomparison Project 6 (CMIP6) models under four Shared Socioeconomic Pathways (SSPs). The results show that the projected daytime and nighttime HWs will impact around 185–492 and 204–555 million people under the selected SSPs, respectively, with the maximum exposure occurring in the Indo-Gigantic Plain. The wide range of populations under different SSPs highlights the sensitivity of the population to future SSP decisions. This emphasizes the importance of reducing greenhouse gas emissions and adopting sustainable urban planning solutions to minimize the potential socioeconomic and health impacts of HWs.

1. Introduction

Heat waves (HWs) are expected to become more frequent and intense in the coming decades due to human-induced climate change (IPCC, 2018; J. Wang et al., 2020; Mukherjee & Mishra, 2018; Vogel et al., 2019; Zscheischler et al., 2018). HWs are projected to have profound effects on human health, with increasing mortality and morbidity across the globe (Gasparrini et al., 2017; Mazdiyasni et al., 2017; Scovronick et al., 2018; Wang et al., 2019). The degree of human exposure to HWs depends not only on the changing climate but also on changes in the size and spatial extent of the population (Jones et al., 2015; Mueller et al., 2014). The human exposure to future HWs is expected to be exacerbated by the simultaneous increases in both temperature and population (King et al., 2018; Trenberth et al., 2015). Therefore, it is important to integrate the influences of

Visualization: Safi Ullah, D. A. Sachindra, Waheed Ullah
Writing – original draft: Safi Ullah, Qinglong You
Writing – review & editing: Qinglong You, Deliang Chen, Amir AghaKouchak, Shichang Kang, Mingcai Li, Panmao Zhai

climate change and the human population, when estimating the exposure to future HWs (Jones et al., 2015). The anticipated human exposure to future HWs is a key component in understanding future vulnerability and risks and is fundamental to sustainable planning and mitigation of the adverse impacts of hot extremes.

South Asia (SA) is one of the world's most populous regions (Figure 1a), with an estimated population of 1.5 billion (Ullah et al., 2020), and its population is expected to reach 2 billion by the mid-21st century (Jones & O'Neill, 2016; Xu et al., 2020). This region is a major hotspot for climate change and future temperature increases (Eckstein et al., 2019). The region has experienced major HWs over the past few decades, which resulted in substantial human and socioeconomic losses. Several modeling studies have projected that this region is highly vulnerable to future HWs and is expected to experience more frequent, intense, and prolonged HWs (Basha et al., 2017; Dong et al., 2021; Mishra et al., 2017; Nasim et al., 2018; Rohini et al., 2019; Saeed et al., 2017; Vogel et al., 2019). Previous studies showed that even a small increase in temperatures significantly enhances the chance of HW-caused mortality in SA (Mazdiyasni et al., 2017). Thus, the increasing prevalence of HWs coupled with the high population density could greatly aggravate the vulnerability of the region in the future. Moreover, the rapid urbanization, high poverty ratio, and low adaptive capacity of this region could further exacerbate the vulnerability to future HW extremes. Thus far, many studies have investigated the underlying mechanisms and tendencies of HWs in SA. However, very little attention has been devoted to determining the exposure of the population to future HWs in this region. The assessment of the future exposure to HWs is critical in devising and prioritizing informed risk reduction and management strategies against potential HW events in SA.

Estimation of the population exposure to future extremes under different climate change and population scenarios requires careful consideration of the climate and population factors. Previous studies have used fixed population estimates (Bouwer, 2013; Smirnov et al., 2016; Sun et al., 2017) and have overlooked the application of explicit population scenarios while quantifying future exposure to climate extremes. For instance, the population exposure was calculated as the frequency of climate extremes in future scenarios multiplied by the current population data. This approach is considered inadequate for projecting the future population exposure, as it is greatly influenced by changes in both the climatic and population factors (Jones et al., 2015; Liu et al., 2020). Moreover, most earlier studies either used individual global/regional climate models or the old versions of the Coupled Model Intercomparison Project (CMIP) models with different combinations of climate change scenarios to quantify the projected exposure to climate extremes (A. Wang et al., 2020; Aadhar & Mishra, 2019; Chen et al., 2020; King et al., 2018; Li et al., 2018; X. Shi et al., 2021; Zhan et al., 2018). However, few studies have employed the recently introduced CMIP6 models to estimate population exposure to climate extremes (Ma & Yuan, 2021; Mondal et al., 2021; Zhao et al., 2021). Given the improvements in CMIP6 models and also the recent socioeconomic pathways (Gidden et al., 2019; O'Neill et al., 2016; Riahi et al., 2017), we believe updating the previous estimates on population exposure is necessary.

In this study, we projected the spatiotemporal changes in the daytime and nighttime HWs in SA and estimated the future population exposure to HW extremes using CMIP6 models under multiple Shared Socioeconomic Pathways (SSPs). We further assessed and quantified the relative contributions of the climate and population to and their compounding effects on the future population exposure in the study region. We separated daytime and nighttime HWs, as warm nights can have significant health impacts and that several studies have highlighted substantial increases in nighttime temperatures in the historical data and/or future projections (Mukherjee & Mishra, 2018; Panda et al., 2017; Ullah et al., 2019; Z. Shi et al., 2021).

2. Data and Methods

2.1. Model Data

The daily maximum (T_{max}) and minimum (T_{min}) temperature outputs of the global climate models (GCMs) were obtained from the CMIP6 data archive (https://esgf-node.llnl.gov/search/cmip6) (Eyring et al., 2016). The details of the selected models are listed in Table 1. It is worth mentioning that most parts of SA experience extreme temperature and HW episodes during the summer season (Khan et al., 2020; Rohini et al., 2019; Ullah et al., 2019). For this reason, we focused on May–September for HW analysis. The GCMs data include data for the historical period (1975–2014) and the future period (2061–2100) under four SSP scenarios, that is, SSP1-2.6, SSP2-4.5, SSP3-7.0, and SSP5-8.5. We chose this period for our study because the projected average tendencies

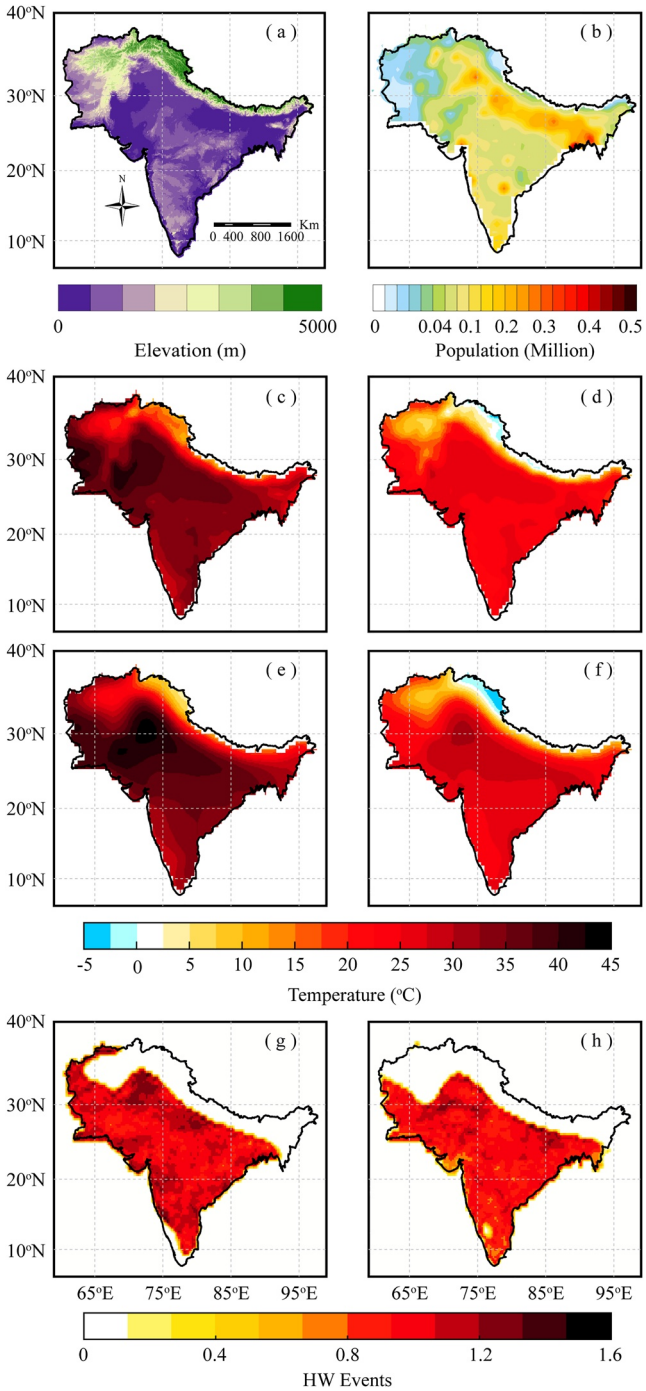

Figure 1. (a) Elevation in South Asia (SA); (b) Spatial distribution of the population in SA in 2000; Spatial distribution of the historical (1975–2014), (c and e) maximum (T_{max}), and (d) & (f) minimum (T_{min}) temperature climatologies, in SA from the Climate Research Unit (CRU) data and the ensemble means of 21 Coupled Model Intercomparison Project 6 (CMIP6) models, respectively; Spatial distribution of the historical mean (1975–2014) (g) daytime and (h) nighttime heat waves (HWs), in SA from the ensemble mean of 21 CMIP6 models.

of T_{max}, T_{min}, and the population density are likely to be higher in SA under the selected SSPs during this period (A. Wang et al., 2020; Liu et al., 2020; Mondal et al., 2021).

It should be noted that scenarios SSP2-4.5 and SSP5-8.5 consist of 21 models while scenarios SSP3-7.0 and SSP1-2.6 consist of 17 and 16 models, respectively. More details about the available SSPs and the selected CMIP6 models for T_{max} and T_{min} are provided in Table 2. The selection of the GCMs was based on the availability of their first simulation variant (r1i1p1f1) for the respective scenarios. The new SSP scenarios of CMIP6 are a combination of socioeconomic development pathways and forcing levels (Keilman, 2020; O'Neill et al., 2016), with an estimated radiative forcing of up to 2.6, 4.5, 7.0, and 8.5 W m^{-2}, under the given specific levels of the greenhouse gas concentrations by the end of the 21st century (Gidden et al., 2019; Riahi et al., 2017). More details about the SSP scenarios are provided by O'Neill et al. (2016). Since the CMIP6 models are available at different spatial resolutions; all of the selected models were regridded to a common 0.5° × 0.5° grid, using the bilinear interpolation technique (Liu et al., 2020; Zhai et al., 2020). In this study, the ensemble means of the selected models were used for the respective scenarios because the multi-model ensemble means are often considered superior to the use of an individual model (A. Wang et al., 2020; Ullah et al., 2020).

2.2. Population Data

The population distribution in the year 2000 and the future projections for 2061–2100 under scenarios SSP1, SSP2, SSP3, and SSP5 were used to estimate the future population exposure to different types of HWs in SA (https://www.cgd.ucar.edu/iam/modeling/spatial-population-scenarios.html) (Jones & O'Neill, 2016). The population datasets were resampled into 0.5° × 0.5° resolution to match the GCMs (A. Wang et al., 2020; Liu et al., 2020). The 2000 population distribution data were combined with the historical period's data to estimate the historical exposure (Chen et al., 2020; Li et al., 2018). The SSP1, SSP2, SSP3, and SSP5 population projections were combined with the respective socioeconomic and forcing scenarios of SSP1-2.6, SSP2-4.5, SSP3-7.0, and SSP5-8.5, respectively, to estimate the potential changes in the population exposure to HWs under each scenario in the study area.

2.3. Bias Correction

For the bias correction, the additive scaling factor technique was used to correct the future projections of the models using the observed data. The additive scaling factor is a commonly used statistical method that facilitates the comparison of observed and simulated impacts during a historical reference period and ensures a continuous transition into the future (Liu et al., 2020). The scaling factor preserves the sensitivities of the GCMs and the underlying trends (Hempel et al., 2013). This method has been widely applied in many climate impact studies (A. Wang et al., 2020; Li et al., 2018; Liu et al., 2020).

For daily T_{max} and T_{min} in each model, a mean correction (MC) additive scale was computed from the difference between the observed and simulated temperatures during 1975–2014. The MC additive scale was then added to the models' future climates to correct the bias.

$$T_{MC} = T_{MP} + (T_{OBS} - T_{MH}), \quad (1)$$

Table 1
Details of the Selected CMIP6 Models

S. No	Model name	Country name	Horizontal resolution (lon × lat)	Reference
1	ACCESS-CM2	Australia	1.9° × 1.3°	Bi et al. (2013)
2	ACCESS-ESM1-5	Australia	1.9° × 1.2°	Law et al. (2017)
3	AWI-CM-1-1-MR	Germany	0.94° × 0.93°	Semmler et al. (2020)
4	BCC-CSM2-MR	China	1.1° × 1.1°	Wu et al. (2019)
5	CanESM5	Canada	2.8° × 2.8°	Swart et al. (2019)
6	CMCC-CM2-SR5	Italy	1.25° × 0.9°	Cherchi et al. (2019)
7	EC-Earth3	Europe	0.7° × 0.7°	Massonnet et al. (2020)
8	EC-Earth3-veg	Europe	0.7° × 0.7°	Wyser et al. (2020)
9	FGOALS-g3	China	2° × 2.3°	Li et al. (2020)
10	GFDL-CM4	USA	2° × 2°	Held et al. (2019)
11	GFDL-ESM4	USA	1.3° × 1.0°	Dunne et al. (2020)
12	INM-CM4-8	Russia	2° × 1.5°	Volodin et al. (2018)
13	INM-CM5-0	Russia	2° × 1.5°	Volodin et al. (2017)
14	IPSL-CM6A-LR	France	2.5° × 1.3°	Boucher et al. (2020)
15	MIROC6	Japan	1.4° × 1.4°	Tatebe et al. (2018)
16	MPI-ESM1-2-HR	Germany	0.9° × 0.9°	Gutjahr et al. (2019)
17	MPI-ESM1-2-LR	Germany	1.9° × 1.9°	Mauritsen et al. (2019)
18	MRI-ESM2-0	Japan	1.1° × 1.1°	Yukimoto et al. (2019)
19	NESM3	China	1.9° × 1.9°	Cao et al. (2018)
20	NorESM2-LM	Norway	2.5° × 1.9°	Seland et al. (2020)
21	NorESM2-MM	Norway	1.25° × 0.9°	Seland et al. (2020)

where T_{MC} and T_{MP} are the corrected and projected temperatures, respectively. The T_{OBS} and T_{MH} are the climatological monthly means of the observed and simulated temperatures, respectively. Similarly, ($T_{OBS} - T_{MH}$) is the scaling factor for the month-to-month changes.

The observed T_{max} and T_{min} datasets of the Climatic Research Unit gridded Time Series (CRU-TS 4.04) with a 0.5° × 0.5° horizontal resolution (Harris et al., 2020) were used to correct the model bias in SA. The time period of the CRU data is from 1975 to 2014, which is in line with the historical period of the models' data.

2.4. Definition of HWs

The HW risk can be quantified using either the daily T_{max} or T_{min} and/or T_{mean}. However, in recent years, the daily T_{max} and T_{min} have been widely used to study daytime and nighttime HW activities in different parts of the world (Cowan et al., 2014; Li et al., 2018; Luo & Lau, 2017; Mukherjee & Mishra, 2018; Raei et al., 2018; Ullah et al., 2019; Zhang et al., 2020). It is argued that daytime HWs pose serious risks to human health; however, the persistent occurrence of nighttime heat stress can further exacerbate human discomfort and pre-existing health conditions (Meehl & Ebaldi, 2004; Mukherjee & Mishra, 2018; Panda et al., 2017). Thus, the occurrence of consecutive hot days and nights has potential implications for human mortality and morbidity.

HWs have no universal definition and can be defined using either percentile or absolute thresholds (You, Jiang, et al., 2017). In this study, we adopted an integrated approach by combining the percentile-based and absolute value-based thresholds to define an HW event in the study area (Dosio et al., 2018; Russo et al., 2017, 2019; Xie et al., 2020). This approach has been used in previous studies to define HW events in the Indo-Pak sub-continent (Rohini et al., 2016, 2019). The percentile-based threshold is defined as the 90th percentile of the T_{max} and T_{min} based on a 5-day window during the historical period (1975–2014) for daytime and nighttime HWs, respectively. The 5-day moving window centered on each calendar day is considered to account for the temporal variability while producing a reasonable sample size for calculating a realistic percentile value. In addition, we used the

Table 2
Details of the Available SSP Scenarios for T_{max} and T_{min} in the Selected CMIP6 Models

		T_{max}					T_{min}				
S. No	Model name	Historical	SSP1-2.6	SSP2-4.5	SSP3-7.0	SSP5-8.5	Historical	SSP1-2.6	SSP2-4.5	SSP3-7.0	SSP5-8.5
1	ACCESS-CM2	✓		✓		✓	✓		✓		✓
2	ACCESS-ESM1-5	✓		✓		✓	✓		✓		✓
3	AWI-CM-1-1-MR	✓	✓	✓	✓	✓	✓	✓	✓	✓	✓
4	BCC-CSM2-MR	✓	✓	✓	✓	✓	✓	✓	✓	✓	✓
5	CanESM5	✓	✓	✓	✓	✓	✓	✓	✓	✓	✓
6	CMCC-CM2-SR5	✓		✓	✓	✓	✓		✓	✓	✓
7	EC-Earth3	✓	✓	✓	✓	✓	✓	✓	✓	✓	✓
8	EC-Earth3-veg	✓	✓	✓	✓	✓	✓	✓	✓	✓	✓
9	FGOALS-g3	✓	✓	✓	✓	✓	✓	✓	✓	✓	✓
10	GFDL-CM4	✓		✓		✓	✓		✓		✓
11	GFDL-ESM4	✓	✓	✓	✓	✓	✓	✓	✓	✓	✓
12	INM-CM4-8	✓	✓	✓	✓	✓	✓	✓	✓	✓	✓
13	INM-CM5-0	✓	✓	✓	✓	✓	✓	✓	✓	✓	✓
14	IPSL-CM6A-LR	✓	✓	✓	✓	✓	✓	✓	✓	✓	✓
15	MIROC6	✓	✓	✓	✓	✓	✓	✓	✓	✓	✓
16	MPI-ESM1-2-HR	✓	✓	✓	✓	✓	✓	✓	✓	✓	✓
17	MPI-ESM1-2-LR	✓	✓	✓	✓	✓	✓	✓	✓	✓	✓
18	MRI-ESM2-0	✓	✓	✓	✓	✓	✓	✓	✓	✓	✓
19	NESM3	✓		✓		✓	✓		✓		✓
20	NorESM2-LM	✓	✓	✓	✓	✓	✓	✓	✓	✓	✓
21	NorESM2-MM	✓	✓	✓	✓	✓	✓	✓	✓	✓	✓

Note. The ✓ sign indicates the availability of the SSP scenario in the respective model for T_{max} and T_{min}.

absolute thresholds of daily climatological $T_{max} \geq 35$°C and $T_{min} \geq 25$°C for daytime and nighttime HWs, respectively. Based on these two thresholds, a daytime (nighttime) HW event is defined by the daily T_{max} (T_{min}) ≥ 90th percentile threshold of the historical period daily climatological T_{max} (T_{min}) of ≥35°C (25°C) for at least 3 consecutive days (nights). These criteria were selected carefully to determine the HW events occurring over the continental plains of SA (Rohini et al., 2016, 2019). The 90th percentile threshold has been widely used by researchers to study HW extremes (Cowan et al., 2014; Liao et al., 2018; Perkins & Alexander, 2013; Ullah et al., 2019). Moreover, the 35°C (25°C) absolute threshold was used to limit the occurrence of daytime (nighttime) HW events over the mountainous region of SA (Rohini et al., 2016, 2019), where the temperature is expected to be well below the adopted threshold (Das & Meher, 2019; Dimri et al., 2018; Ullah et al., 2020).

2.5. Estimation of Population Exposure to HWs

The population exposure is the number of HW events multiplied by the number of people exposed to that outcome in each grid cell (Jones et al., 2015; Jones & O'Neill, 2016). The change in future population exposure was measured with reference to the historical period. To minimize the interannual variations, we used the 40-year mean of HWs and population to calculate the exposure to each type of HW during both the historical and future periods (Batibeniz et al., 2020; Liu et al., 2020). The 40-year average exposure was calculated for each grid cell using Equation 2.

$$E_P = \frac{\sum_{i=1}^{40} \mathrm{HW}_i \times P}{40}, \quad (2)$$

where E_P is the 40-year mean population exposure (person-events), i is the ith year of the study period, HW_i is the annual number of HW events, and P is the simulated population (number of people).

2.6. Estimation of the Relative Roles of the Exposure Factors

To determine the relative contributions of the climatic and population factors to the HWs exposure, we decomposed the changes in the population exposure into the climatic driver (temperature), effects of population increase, and their compounding effects, with the sum representing the overall exposure (Jones et al., 2015; Rohat et al., 2019). The effects of the population were calculated by keeping the climate constant while using the number of HW events in the historical period multiplied by the population in each SSP scenario. Similarly, the climate effects were calculated by holding the population constant and using the number of HW events in each SSP scenario multiplied by the population in the historical period. The compounding effects of both were estimated to identify the areas with continuous population growth and frequent HWs under future climate change. The changes in the population exposure were decomposed using Equation 3.

$$\Delta E_P = \mathrm{HW}_H \times \Delta P + P_H \times \Delta \mathrm{HW} + \Delta P \times \Delta \mathrm{HW}, \tag{3}$$

where ΔE_P is the total change in the population exposure (people/event), HW_H is the number of HWs in the historical period (events), ΔP is the change in the population from the historical period to the future period (people), P_H is the population in the historical period (person), and ΔHW is the change in the number of HWs from the historical period to the future period (events). Thus, $HW_H \times \Delta P$ is the population effect, $P_H \times \Delta$HW is the climatic effect, and $\Delta P \times \Delta$HW is the compounding effect (or interaction) between the climate change and population change.

3. Results and Discussion

3.1. Changes in Historical Population, Temperature, and HWs

The spatial distribution of historical population indicates that the highest population density occurs on the Indo-Gigantic Plains (IGP), followed by the southeastern parts of India and the northwestern parts of the Pak-Afghan border (Figure 1b). The IGP extends from the northern-central parts of the Indian Subcontinent to its extreme northeastern parts (Biemans et al., 2019), mainly including the northeastern parts of Pakistan, northern India, and Bangladesh. This region is located among the three major river basins in SA, namely the Brahmaputra, Ganges, and Indus rivers (Biemans et al., 2019; Pathak et al., 2017; Xu et al., 2020). It should be noted that the IGP is the most densely populated region of the Indian Sub-continent (Im et al., 2017; Kaskaoutis et al., 2011) due to its fertile land, water availability, and high livelihood opportunities (Biemans et al., 2019; Viviroli et al., 2020). The complex topography, diverse climatology, distinct geographical location, and fragile socioeconomic conditions further exacerbate the vulnerability of this region to climate change and its extremes (Ramachandran & Kedia, 2013; Sen et al., 2017).

In terms of observed and GCM simulated temperature climatologies, the historical distribution of the maximum (T_{max}) and minimum (T_{min}) temperatures exhibits a warming pattern in the central parts of SA, with a maximum intensity along the Indo-Pak border (Figures 1c–1f). This region has a hot and dry climate with a desert landscape, making it more susceptible to climate extremes. Due to its complex topographic and climatic features, the region is considered to be a climate change-prone region. Moreover, the eastern parts of India and the southwestern parts of Pakistan and Afghanistan also have a warm climate. In contrast, the Hindukush Karakorum and Himalaya (HKH) ranges have the lowest temperatures, which is attributed to their cold and humid climate. It is worth stating that the spatial patterns of both the observed and simulated climatologies are similar; however, the intensity of GCMs climatologies is slightly higher (lower) than those of the observed climatologies over the plains (mountainous) region of SA. Given the warm and cold biases in the historical simulations of GCMs, we could expect similar patterns in their respective future projections, which need to be bias-corrected. Thus, the future projections of all CMIP6 GCMs were bias-corrected prior to their use for HWs analysis as described in the Methods Section.

The results further show that the frequency of historical daytime and nighttime HWs is high throughout the plains areas of SA. However, the highest number of HW events occurred in the IGP, the southeastern coastal belt,

and the southwestern parts of Afghanistan (Figures 1g–1h). This indicates that these regions have experienced frequent HW events in recent decades. It is vital to mention that these parts of SA are listed among the hottest regions of the world and are highly exposed to frequent HWs (Mishra et al., 2020; Mueller et al., 2014; Ullah et al., 2019; You, Ren, et al., 2017). In addition, these regions have had a high population density in the historical period, highlighting their fragile socioeconomic conditions and susceptibility to climate change-induced extremes. Interestingly, the HKH region has not experienced any HW event in the historical period, which is attributed to the low-temperature tendency in the mountainous parts of SA. Moreover, the absence of HWs in the HKH region could be due to the criteria used in this study for defining HW events.

3.2. Changes in Future HWs

The relative change in HWs indicates that the SA region is expected to experience an increase in the daytime and nighttime HWs, with the highest number of HW events occurring in the central, northwestern, southern, and northeastern parts under all of the SSP scenarios, relative to the historical period (Figures 2a–2h). The distribution of the future HWs exhibits a dipolar pattern, with the maximum number of daytime HWs occurring in the northwestern parts of Pakistan and the highest number of nighttime HWs occurring in southern Pakistan, northeastern India, and Bangladesh. The rapid increase in the number of HW events in the northwestern parts of Pakistan can be attributed to an elevation-dependent increase in temperature since these areas are located at relatively high altitudes. Several studies have reported more warming in the northwestern parts of SA than in the low-lying plains areas (Pepin et al., 2015; Shen et al., 2021; You et al., 2020). Interestingly, the Indo-Pak border is expected to have consistent increases in both the number of daytime and nighttime HWs during 2061–2100, relative to the historical period (1975–2014). This part of SA has a desert environment with a hot and dry climate and thus experiences recurrent HW episodes. The frequent occurrence of HWs along the Pak-India border affirms the increasing trends of T_{max} and T_{min} in the coming decades.

Surprisingly, the number of daytime HWs is expected to decrease in the southwestern parts of Pakistan under scenario SSP1-2.6, followed by SSP2-4.5, and SSP3-7.0, relative to the historical period. Similarly, the number of nighttime HWs is likely to decrease in the southwestern parts of Pakistan and southern and eastern coastal regions of India under scenarios SSP1-2.6 and SSP2-4.5. The spatial extent of the decrease in the number of nighttime HWs is higher than that of daytime HWs. However, the area showing less HWs in the future is significantly smaller than the areas pointing to more HWs in the future. It should be noted that the HKH region is not prone to extreme HWs compared to some other parts of the region, due to the low-temperature tendency in this region (see also the absolute temperature thresholds for the HW definition in the Methods Section).

In terms of frequency, the number of nighttime HWs is likely to be higher than the number of daytime HWs under most of the selected scenarios. This uneven pattern of HWs can be attributed to the asymmetric increases in T_{max} and T_{min}, as recent studies anticipate that T_{min} is likely to increase at a faster rate than T_{max} (Kang et al., 2010; Ullah et al., 2020), which would affect the frequency of their extremes in the study area. Moreover, the spatial coverage of the future HWs indicates that the daytime HWs will occur in a larger area than the nighttime HWs under scenarios SSP1-2.6, SSP2-4.5, and SSP3-7.0. Overall, the results suggest that the numbers and the spatial coverages of the daytime (nighttime) HWs are projected to be higher under scenario SSP5-8.5, followed by SSP2-4.5, SSP3-7.0, and SSP1-2.6 (SSP5-8.5, SSP3-7.0, SSP2-4.5, and SSP1-2.6), relative to the historical period.

The box and whisker plot shows the spread of changes in the regional mean number of daytime and nighttime HWs under the selected SSP scenarios, relative to the historical period (Figure 2i). The daytime HWs exhibit higher maxima values under all the SSPs relative to the historical period, suggesting that the study region will experience frequent daytime HWs in the future. The higher maxima values of daytime HWs can also be affirmed from the spatial pattern of HWs since most parts of the SA are likely to be dominated by frequent HWs during the daytime. Moreover, the nighttime HWs have high interquartile ranges (IQR) under the selected SSPs; however, their minima values are slightly lower (≤ 0) than daytime HWs. The lower minima of the nighttime HWs can be attributed to their decreasing trend since the southern and eastern parts of SA will experience a relatively more decline in nighttime HWs than daytime HWs during the study period. Relative to the daytime HWs, the nighttime HWs have higher maxima values under SSP3-7.0 and SSP5-8.5 scenarios, indicating a relatively sharp increase in HW events at nighttime than daytime under the said scenarios. These results can be confirmed from the spatial pattern of HWs under SSP3-7.0 and SSP5-8.5, where more HWs can be seen at nighttime than daytime, particularly in the central and northeastern parts of SA. Overall, the number and spread of daytime (nighttime) HWs

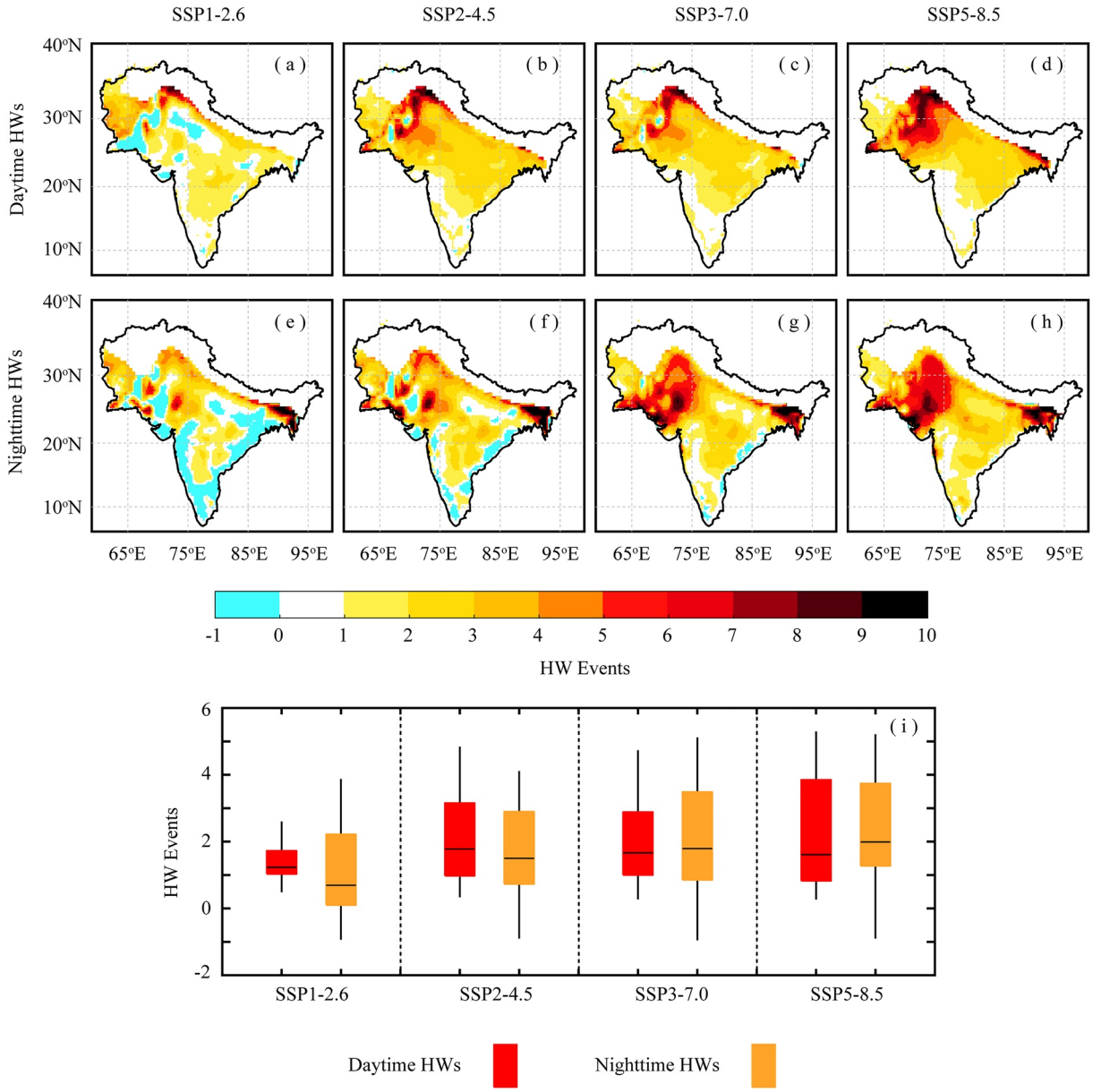

Figure 2. Projected changes in the future (2061–2100) (a–d) daytime and (e–h) nighttime heat waves (HWs) in South Asia from the multi-model ensemble means under different Shared Socioeconomic Pathways (SSPs), relative to the historical period (1975–2014); (i) Projected regional mean changes in the daytime and nighttime HWs. The box plots indicate the spatial spread of regional mean values for daytime and nighttime HWs under the selected SSPs.

will be higher under SSP5-8.5, followed by SSP2-4.5, SSP3-7.0, and SSP1-2.6 (SSP5-8.5, followed by SSP3-7.0, SSP2-4.5, and SSP1-2.6) scenarios.

3.3. Estimation of Population Exposure to Future HWs

The spatial pattern of the relative population exposure to future daytime and nighttime HWs in SA exhibits a high spatial variability under multiple SSP scenarios during 2061–2100 (Figures 3a–3h). The regions with higher population exposures (0.25–2.25 million people-event) to HWs are mainly located in the northern parts of SA, comprising the IGP region. Within the IGP region, the highest degree of population exposure will occur along the northwestern Indo-Pak border and in northeastern India and Bangladesh. It should be noted that these parts of SA contain the largest metropolitan cities, including Lahore, Faisalabad, Amritsar, Delhi, Patna, Kolkata,

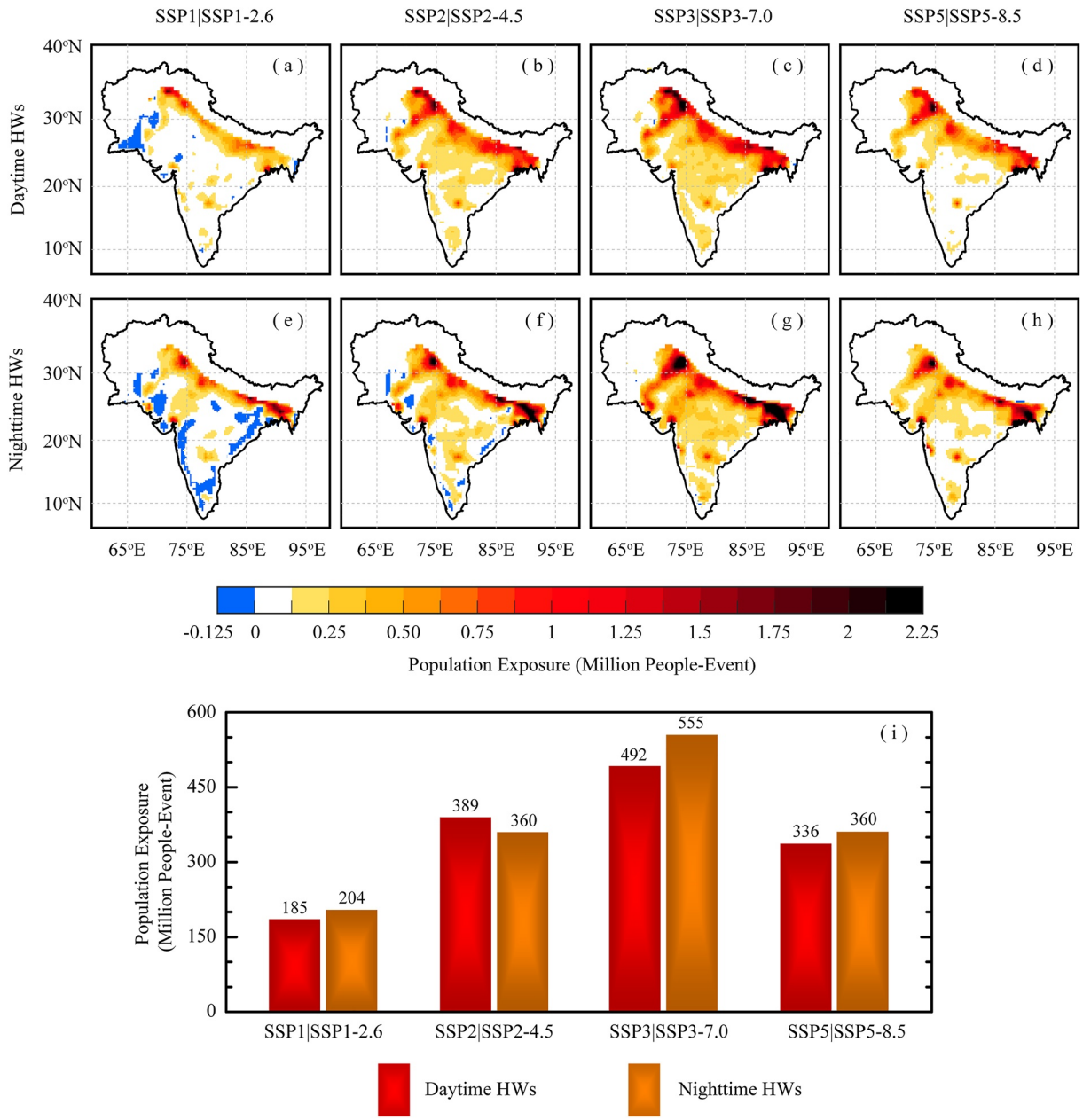

Figure 3. Projected population exposure to future (2061–2100) (a–d) daytime and (e–h) nighttime heat waves (HWs) in Suth Asia from the multi-model ensemble means under different Shared Socioeconomic Pathways (SSP) scenarios, relative to the historical period (1975–2014). (i) Projected regional sums of population exposure to daytime and nighttime HWs (i.e., values above each bar in Figure 3i indicate the regional sums of population exposure to daytime and nighttime HWs under the corresponding SSP scenarios).

and Dhaka. It should also be noted that the IGP is one of the world's most populated regions and its rising rate of population will continue in the future (A. Wang et al., 2020; Im et al., 2017). Moreover, this region is highly sensitive to climate change due to its physical and socioeconomic conditions (Biemans et al., 2019; Viviroli et al., 2020). Thus, the increase in population accompanied by the prevailing occurrence of HWs may exacerbate the population exposure and the magnitudes of the potential risks to human lives and their socioeconomic assets in the region (Mishra et al., 2020). Moreover, the central parts of India will also be exposed to future daytime and nighttime HWs under most of the SSP scenarios (0.125–1.25 million people-event). The population exposure in central India could be due to the compounding effects of climate change and population since this part of SA has a relatively low population and experiences a relatively lower number of HW events.

In contrast, the southwestern parts of Pakistan and India, and the southern and eastern coastal belts of the Indian Ocean will experience a decrease (−0.125 million people-event) in population exposure to future HWs under scenarios SSP1|SSP1-2.6 and SSP2|SSP2-4.5. The estimated decrease in population exposure will be larger for nighttime HWs than daytime HWs. The resultant decrease in the extent of the population exposure in these regions can be attributed to the decreasing trend of future HWs, as we find that these regions predominantly exhibit a pattern of decreasing daytime and nighttime HWs in the future. It should be noted that the above-mentioned areas will experience a positive shift in population exposure under scenarios SSP3|SSP3-7.0 and SSP5|SSP5-8.5, which could be related to the effects of population growth and high radiative forcing embedded in these scenarios. Interestingly, all of Afghanistan, the southern belt of Pakistan, the HKH ranges, and the southern parts of India will not witness a large extent of population exposure, which could be due to the absence of future HW events in these regions.

The results further demonstrate that the degree of population exposure and its spatial extent is expected to be higher for nighttime HWs than for daytime HWs under the selected scenarios, relative to the historical period. The heterogeneity in the degree and extent of the population exposure to the different types of HWs could be possible outcomes for the maximum number of nighttime HW events in the study area. Moreover, the asymmetric increases in T_{max} and T_{min} may influence the degree of exposure because it is projected that T_{min} will increase at a higher rate than T_{max} in the study region (Ullah et al., 2020), which would intensify the occurrence of nighttime HWs than daytime in the future. Furthermore, the highest degree of population exposure to daytime and nighttime HWs occurs under scenario SSP3|SSP3-7.0, followed by SSP2|SSP2-4.5, SSP5|SSP5-8.5, and SSP1|SSP1-2.6. The scale of the exposure under these scenarios can be attributed to the combined effects of population, urbanization, and radiative forcing since the selected scenarios are embedded with a sharp rise in population and rapid urbanization coupled with a high radiative forcing under the given level of greenhouse gas concentrations (Gao & O'Neill, 2020; Jing et al., 2020; Jones & O'Neill, 2016).

The regional sums indicate that there will be an increase in population exposure to daytime and nighttime HWs under all of the SSP scenarios with the highest exposure under scenario SSP3|SSP3-7.0, followed by SSP2|SSP2-4.5, SSP5|SSP5-8.5, and SSP1|SSP1-2.6 (Figure 3i). The degree of the population exposure to daytime HWs is higher under scenarios SSP2|SSP2-4.5 while that of the nighttime HWs is higher under scenarios SSP1|SSP1-2.6, SSP3|SSP3-7.0, and SSP5|SSP5-8.5. The differences in the population exposures to daytime and nighttime HWs under the selected scenarios could be the result of the variations in the numbers of daytime and nighttime HWs. Relative to the historical period, the total estimated population exposure to daytime HWs in SA is 185, 389, 492, and 336 million people-event under scenarios SSP1|SSP1-2.6, SSP2|SSP2-4.5, SSP3|SSP3-7.0, and SSP5|SSP5-8.5, respectively. Similarly, the total population exposure to nighttime HWs is 204, 360, 555, and 360 million people-event under scenarios SSP1|SSP1-2.6, SSP2|SSP2-4.5, SSP3|SSP3-7.0, and SSP5|SSP5-8.5, respectively. These results are in line with the spatial distributions of the population exposures to daytime and nighttime HWs under the selected SSP scenarios.

Though the present study estimated future population exposure to daytime and nighttime HWs in SA; however, it has some limitations that need to be addressed in the forthcoming studies. This study did not employ the socioeconomic and demographic characteristics of the population (i.e., income, education level, and age), which may affect the degree of risk posed by HWs in the study region (Chambers, 2020; Gasparrini et al., 2017; Jones et al., 2015; Watts et al., 2019, 2021). Moreover, this study used the total population of the study area, without considering the urban and rural differences, which may also affect the extent of exposure, as urban sites are likely to be at higher risk of HWs (Batibeniz et al., 2020; Rohat et al., 2019; Scovronick et al., 2018; Wang et al., 2019). We believe that future studies estimating population exposure will be based on more refined socioeconomic and demographic classifications. Currently, many studies are focusing on exposure to climate extremes but there is no uniform definition of exposure yet. Some studies have used the method of multiplying extreme events and population numbers to estimate the population exposure to climate extremes (Batibeniz et al., 2020; Jones et al., 2015; Mondal et al., 2021). Some studies have defined exposure as the area experiencing climate extremes exceeding the danger threshold for a given time period (Sun et al., 2019; Zhang et al., 2018), while some have considered the intensity-area-duration method of disaster events to reflect the changes in exposure (A. Wang et al., 2020; Wen et al., 2019; Zhao et al., 2021). Due to the different definitions, the estimation of population exposure and the socioeconomic impacts of climate extremes are also different. Therefore, there is a need for a more scientific,

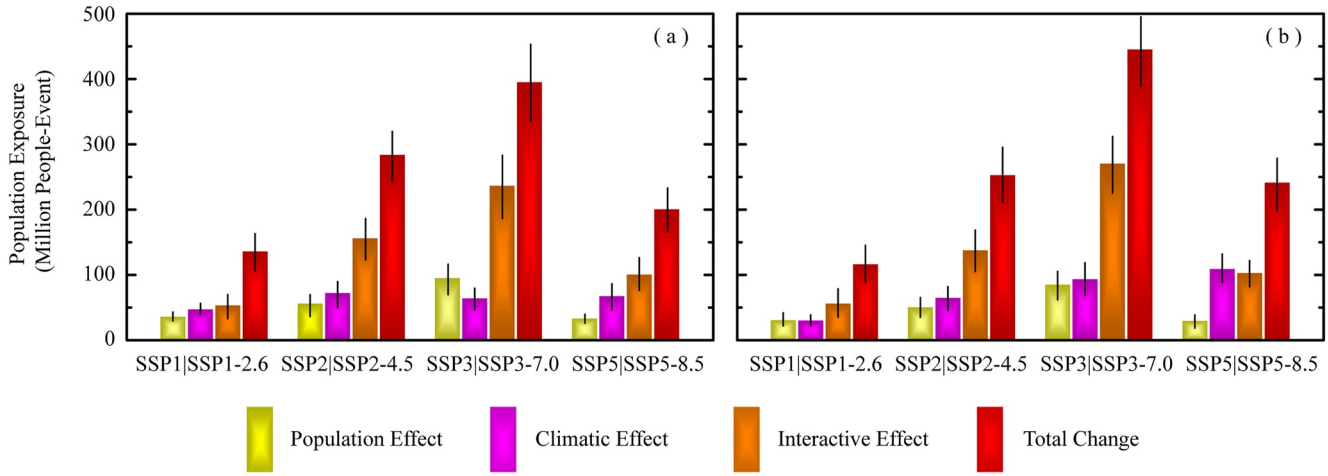

Figure 4. Decomposition of the changes in the effects of the exposure factors and their sums on (a) daytime and (b) nighttime HWs in the future (2061–2100) under different SSP scenarios, relative to the historical period (1975–2014). The error bars indicate the standard deviations of the respective exposure factors.

rational, sound, and uniform definition of population exposure to extreme events that takes into account the hazard, exposure, and vulnerability aspects to adequately reflect the socioeconomic impacts of disasters.

3.4. Changes in Exposure Factors

In terms of the underlying roles of the exposure factors, the interactions between population and climatic factors are likely to play a more prominent and intensifying role in escalating population exposure to HWs in SA than their individual effects. The results show that the compounding effects of both drivers will exacerbate population exposure to both daytime and nighttime HWs under SSP3|SSP3-7.0, followed by SSP2|SSP2-4.5, SSP5|SSP5-8.5, and SSP1|SSP1-2.6 scenarios (Figures 4a and 4b). Overall, the relative contribution of the compounding effects on population exposure to daytime (night-time) HWs will be 236, 156, 100, and 53 (270, 137, 103, and 56) million people-event, under SSP3|SSP3-7.0, SSP2|SSP2-4.5, SSP5|SSP5-8.5, and SSP1|SSP1-2.6 scenarios, respectively. This indicates that the combination of anthropogenic and climatic factors is likely to be more significant in the future and may result in the frequent occurrence of daytime and nighttime HWs, with serious consequences for the study region. The major role of the compounding effects in population exposure to HWs can be attributed to the concurrent impacts of high population density and rapid urbanization coupled with high concentrations of greenhouse gas emissions under the selected SSP scenarios. It should be noted that the SSP2, SSP3, and SSP5 are embedded with the effects of high urbanization rate, rapid population growth, and high radiative forcing, respectively (Jones & O'Neill, 2016; Murakami & Yamagata, 2019; Riahi et al., 2017).

Irrespectively, the contribution of the climate in population exposure to daytime HWs is greater under SSP2|SSP2-4.5 (72 million people-event) than SSP3|SSP3-7.0 (64 million people-event) and SSP5|SSP5-8.5 (67 million people-event). The higher climatic effect on population exposure to daytime HWs under SSP2|SSP2-4.5 could be linked to a slight increase in the exposed area in southern parts of India (Figures 2b and 3b). In contrast, the role of population effects in escalating the exposure to daytime HWs is greater than that of the climatic effects under the SSP3|SSP3-7.0 scenario, which can be attributed to the inclusion of the population influence since this scenario is considered to have a high population growth than the rest of the SSPs (Chen et al., 2020; Jones & O'Neill, 2016).

In the case of nighttime HWs, the role of climate in population exposure to nighttime HWs is slightly higher than that of both drivers under SSP5|SSP5-8.5 (109 million people-event), which could be the possible outcome of radiative forcing and concentration of the greenhouse gas emissions, since this scenario has high radiative forcing and greenhouse gas emissions effects (Gidden et al., 2019; O'Neill et al., 2016; Riahi et al., 2017). Similarly, the contribution of climatic effects (93 million people-event) in population exposure to nighttime is slightly higher than the population effects (85 million people-event) under SSP3|SSP3-7.0, which can be attributed to the joint

effects of high HWs number and population since this scenario is embedded with a high population growth rate (Batibeniz et al., 2020; Jones & O'Neill, 2016; Liu et al., 2020).

It should be noted that the current GCMs do not fully resolve the climatic effects of urbanization. However, the SSP scenarios considered the effects of urbanization in terms of greenhouse gas emissions, which influence the large-scale climate resolved by the GCMs. The new SSPs are developed by integrating climate forcing and socioeconomic conditions (Gidden et al., 2019; O'Neill et al., 2016). For instance, SSP2-4.5 and SSP3-7.0 are embedded with the effects of high urbanization rate and rapid population growth, respectively (Gao & Pesaresi, 2021; Jones & O'Neill, 2016; Riahi et al., 2017). Thus, the influence of urbanization and population coupled with radiative forcing could affect the large-scale climatic conditions resolved by the CMIP6 GCMs. Similar results were also reported in this study, where urbanization and population coupled with radiative forcing have significant impacts on HWs and population exposure under SSP2-4.5, SSP3-7.0, and SSP5-8.5.

Our results are in line with the results of previous studies (Batibeniz et al., 2020; Chen et al., 2020; Jones et al., 2015; Liu et al., 2020) conducted in different parts of the world, including our study region. Overall, the results suggest that the population of the study region is highly vulnerable to the risks imposed by the projected daytime and nighttime HWs under the selected SSPs. Moreover, the increasing role of the joint effects of anthropogenic and climatic factors in population exposure under different SSPs highlights the need for proper population planning, sustainable urban planning, the mitigation of greenhouse gas emissions, and adaptation measures in order to minimize human exposure to HWs in the study region.

4. Conclusions

In this study, the projected population exposure in southern Asia to daytime and nighttime HWs during 2061–2100 under multiple SSP scenarios was estimated, relative to the historical period. It was found that the study area is most likely to experience a rise in the numbers of daytime and nighttime HWs, with the highest frequency occurring in the central, northwestern, southern, and northeastern parts of SA under all of the SSP scenarios. The frequency and spatial extent of the nighttime HWs will be higher than those of the daytime HWs under scenario SSP5-8.5, followed by SSP3-7.0, SSP2-4.5, and SSP1-2.6. Similarly, the projected population exposure to HWs is likely to be high in the IGP and central parts of India under all of the SSP scenarios. The estimated exposure and its extent will be greater for the nighttime HWs than for the daytime HWs under scenario SSP3|SSP3-7.0, followed by SSP2|SSP2-4.5, SSP5|SSP5-8.5, and SSP1|SSP1-2.6. In terms of relative importance, the projected changes in the population exposure to all types of HWs in SA are mainly influenced by the compounding effects of both drivers, followed by climatic change and projected population increases under the selected SSP scenarios. The prominent role of the combined effects of anthropogenic and climatic factors in population exposure under the different SSP scenarios highlights the need for reducing anthropogenic greenhouse gas emissions, sustainable urban planning, and climate change adaptation measures in order to minimize human exposure to future HWs.

Acknowledgments
This study is supported by the Research Fund for International Young Scientists of the National Natural Science Foundation of China (42150410381), National Natural Science Foundation of China (41971072 and 41771069) and the Chinese Academy of Sciences (XDA2006040103). The authors acknowledge the World Climate Research Programme's (WCRP) Working Group on Coupled Modeling (WGCM), which is responsible for CMIP. The authors are thankful to the climate modeling groups (listed in Table 1 of this paper) for producing and making available their CMIP6 model outputs. The authors acknowledge the developers of the CRU data for providing gridded temperature datasets. The first author also acknowledges the Shanghai Local (Municipal) Government for providing financial assistance under the Shanghai Super Postdoctoral Fellowship Program.

Conflict of Interest

The authors declare no conflicts of interest relevant to this study.

Data Availability Statement

All CMIP6 model simulations and CRU data are available at https://esgf-node.llnl.gov/projects/cmip6 and https://crudata.uea.ac.uk/cru/data/hrg/, respectively. The population data are available at https://www.cgd.ucar.edu/iam/modeling/spatial-population-scenarios.html.

References

Aadhar, S., & Mishra, V. (2019). A substantial rise in the area and population affected by dryness in South Asia under 1.5°C, 2.0°C and 2.5°C warmer worlds. *Environmental Research Letters*, *14*(11), 1–20. https://doi.org/10.1088/1748-9326/ab4862

Basha, G., Kishore, P., Ratnam, M. V., Jayaraman, A., Kouchak, A. A., Ouarda, T. B. M. J., & Velicogna, I. (2017). Historical and projected surface temperature over India during the 20th and 21st century. *Scientific Reports*, *7*(1), 1–10. https://doi.org/10.1038/s41598-017-02130-3

Batibeniz, F., Ashfaq, M., Diffenbaugh, N. S., Key, K., Evans, K. J., Turuncoglu, U. U., & Önol, B. (2020). Doubling of U.S. population exposure to climate extremes by 2050. *Earth's Future*, *8*(4), 1–14. https://doi.org/10.1029/2019ef001421

Bi, D., Dix, M., Marsland, S. J., O'Farrell, S., Rashid, H., Uotila, P., et al. (2013). The ACCESS coupled model: Description, control climate and preliminary validation. *Australian Meteorological and Oceanographic Journal*, *63*, 1–24. https://doi.org/10.22499/2.6301.004
Biemans, H., Siderius, C., Lutz, A. F., Nepal, S., Ahmad, B., Hassan, T., et al. (2019). Importance of snow and glacier meltwater for agriculture on the Indo-Gangetic plain. *Nature Sustainability*, *2*(7), 594–601. https://doi.org/10.1038/s41893-019-0305-3
Boucher, O., Servonnat, J., Albright, A. L., Aumont, O., Balkanski, Y., Bastrikov, V., et al. (2020). Presentation and evaluation of the IPSL-CM6A-LR climate model. *Journal of Advances in Modeling Earth Systems*, *12*(7), 1–52. https://doi.org/10.1029/2019ms002010
Bouwer, L. M. (2013). Projections of future extreme weather losses under changes in climate and exposure. *Risk Analysis*, *33*(5), 915–930. https://doi.org/10.1111/j.1539-6924.2012.01880.x
Cao, J., Wang, B., Yang, Y. M., Ma, L., Li, J., Sun, B., et al. (2018). The NUIST Earth system model (NESM) version 3: Description and preliminary evaluation. *Geoscientific Model Development*, *11*(7), 2975–2993. https://doi.org/10.5194/gmd-11-2975-2018
Chambers, J. (2020). Global and cross-country analysis of exposure of vulnerable populations to heatwaves from 1980 to 2018. *Climatic Change*, *163*(1), 539–558. https://doi.org/10.1007/s10584-020-02884-2
Chen, H., Sun, J., & Li, H. (2020). Increased population exposure to precipitation extremes under future warmer climates. *Environmental Research Letters*, *15*(3), 1–11. https://doi.org/10.1088/1748-9326/ab751f
Cherchi, A., Fogli, P. G., Lovato, T., Peano, D., Iovino, D., Gualdi, S., et al. (2019). Global mean climate and main patterns of variability in the CMCC-CM2 coupled model. *Journal of Advances in Modeling Earth Systems*, *11*(1), 185–209.
Cowan, T., Purich, A., Perkins, S., Pezza, A., Boschat, G., & Sadler, K. (2014). More frequent, longer, and hotter heat waves for Australia in the twenty-first century. *Journal of Climate*, *27*(15), 5851–5871. https://doi.org/10.1175/jcli-d-14-00092.1
Das, L., & Meher, J. K. (2019). Drivers of climate over the Western himalayan region of India: A review. *Earth-Science Reviews*, *198*, 1–15. https://doi.org/10.1016/j.earscirev.2019.102935
Dimri, A. P., Kumar, D., Choudhary, A., & Maharana, P. (2018). Future changes over the himalayas: Mean temperature. *Global and Planetary Change*, *162*, 235–251. https://doi.org/10.1016/j.gloplacha.2018.01.014
Dong, Z., Wang, L., Sun, Y., Hu, T., Limsakul, A., Singhruck, P., & Pimonsree, S. (2021). Heatwaves in southeast Asia and their changes in a warmer world. *Earth's Future*, *9*(7), 1–13. https://doi.org/10.1029/2021ef001992
Dosio, A., Mentaschi, L., Fischer, E. M., & Wyser, K. (2018). Extreme heat waves under 1.5 and 2 degree global warming. *Environmental Research Letters*, *13*(4), 1–10. https://doi.org/10.1088/1748-9326/aab827
Dunne, J. P., Horowitz, L. W., Adcroft, A. J., Ginoux, P., Held, I. M., John, J. G., et al. (2020). The GFDL Earth system model version 4.1 (GFDL-ESM 4.1): Overall coupled model description and simulation characteristics. *Journal of Advances in Modeling Earth Systems*, *12*(11), 1–56. https://doi.org/10.1029/2019ms002015
Eckstein, D., Hutfils, M.-L., & Winges, M. (2019). Global climate risk index 2019: Who suffers most from extreme weather events?
Eyring, V., Bony, S., Meehl, G. A., Senior, C. A., Stevens, B., Stouffer, R. J., & Taylor, K. E. (2016). Overview of the coupled model intercomparison project phase 6 (CMIP6) experimental design and organization. *Geoscientific Model Development*, *9*(5), 1937–1958. https://doi.org/10.5194/gmd-9-1937-2016
Gao, J., & O'Neill, B. C. (2020). Mapping global urban land for the 21st century with data-driven simulations and shared socioeconomic pathways. *Nature Communications*, *11*(1), 1–12. https://doi.org/10.1038/s41467-020-15788-7
Gao, J., & Pesaresi, M. (2021). Downscaling SSP-consistent global spatial urban land projections from 1/8-degree to 1-km resolution 2000–2100. *Scientific Data*, *8*(1), 1–9. https://doi.org/10.1038/s41597-021-01052-0
Gasparrini, A., Guo, Y., Sera, F., Vicedo-Cabrera, A. M., Huber, V., Tong, S., et al. (2017). Projections of temperature-related excess mortality under climate change scenarios. *The Lancet Planetary Health*, *1*(9), 360–367.
Gidden, M. J., Riahi, K., Smith, S. J., Fujimori, S., Luderer, G., Kriegler, E., et al. (2019). Global emissions pathways under different socioeconomic scenarios for use in CMIP6: A dataset of harmonized emissions trajectories through the end of the century. *Geoscientific Model Development*, *12*(4), 1443–1475. https://doi.org/10.5194/gmd-12-1443-2019
Gutjahr, O., Putrasahan, D., Lohmann, K., Jungclaus, J. H., Von Storch, J. S., Brüggemann, N., et al. (2019). Max planck institute Earth system model (MPI-ESM1.2) for the high-resolution model intercomparison project (HighResMIP). *Geoscientific Model Development*, *12*(7), 3241–3281. https://doi.org/10.5194/gmd-12-3241-2019
Harris, I., Osborn, T. J., Jones, P., & Lister, D. (2020). Version 4 of the CRU TS monthly high-resolution gridded multivariate climate dataset. *Scientific Data*, *7*(1), 1–18. https://doi.org/10.1038/s41597-020-0453-3
Held, I. M., Guo, H., Adcroft, A., Dunne, J. P., Horowitz, L. W., Krasting, J., et al. (2019). Structure and performance of GFDL's CM4.0 climate model. *Journal of Advances in Modeling Earth Systems*, *11*(11), 3691–3727. https://doi.org/10.1029/2019ms001829
Hempel, S., Frieler, K., Warszawski, L., Schewe, J., & Piontek, F. (2013). A trend-preserving bias correction – The ISI-MIP approach. *Earth System Dynamics Discussions*, *4*(1), 49–92. https://doi.org/10.5194/esd-4-219-2013
Im, E. S., Pal, J. S., & Eltahir, E. A. B. (2017). Deadly heat waves projected in the densely populated agricultural regions of South Asia. *Science Advances*, *3*(8), 1–8. https://doi.org/10.1126/sciadv.1603322
IPCC. (2018). *Global warming of 1.5°C. Genva, Switzerland*. Geneva, Switzerland: Intergovernamental Panel on Climate Change.
Jing, C., Tao, H., Jiang, T., Wang, Y., Zhai, J., Cao, L., & Su, B. (2020). Population, urbanization and economic scenarios over the belt and road region under the shared socioeconomic pathways. *Journal of Geographical Sciences*, *30*(1), 68–84. https://doi.org/10.1007/s11442-020-1715-x
Jones, B., & O'Neill, B. C. (2016). Spatially explicit global population scenarios consistent with the shared socioeconomic pathways. *Environmental Research Letters*, *11*(8), 1–11. https://doi.org/10.1088/1748-9326/11/8/084003
Jones, B., O'Neill, B. C., Mcdaniel, L., Mcginnis, S., Mearns, L. O., & Tebaldi, C. (2015). Future population exposure to US heat extremes. *Nature Climate Change*, *5*(7), 652–655. https://doi.org/10.1038/nclimate2631
Kang, S., Xu, Y., You, Q., Pepin, N., Yao, T., & Fl, W. (2010). Review of climate and cryospheric change in the tibetan plateau. *Environmental Research Letters*, *5*, 1–8. https://doi.org/10.1088/1748-9326/5/1/015101
Kaskaoutis, D. G., Kharol, S. K., Sinha, P. R., Singh, R. P., Badarinath, K. V. S., Mehdi, W., & Sharma, M. (2011). Contrasting aerosol trends over South Asia during the last decade based on MODIS observations. *Atmospheric Measurement Techniques Discussions*, *4*(4), 5275–5323.
Keilman, N. (2020). Modelling education and climate change. *Nature Sustainability*, *3*, 497–498. https://doi.org/10.1038/s41893-020-0515-8
Khan, N., Shahid, S., Ahmed, K., Wang, X., Ali, R., Ismail, T., & Nawaz, N. (2020). Selection of GCMs for the projection of spatial distribution of heat waves in Pakistan. *Atmospheric Research*, *233*(10), 1–14. https://doi.org/10.1016/j.atmosres.2019.104688
King, A. D., Donat, M. G., Lewis, S. C., Henley, B. J., Mitchell, D. M., Stott, P. A., et al. (2018). Reduced heat exposure by limiting global warming to 1.5°C. *Nature Climate Change*, *8*, 549–551. https://doi.org/10.1038/s41558-018-0191-0
Law, R. M., Ziehn, T., Matear, R. J., Lenton, A., Chamberlain, M. A., Stevens, L. E., et al. (2017). The carbon cycle in the Australian community climate and earth system simulator (ACCESS-ESM1) – Part 1: Model description and pre-industrial simulation. *Geoscientific Model Development*, *10*(7), 2567–2590. https://doi.org/10.5194/gmd-10-2567-2017

Li, D., Zhou, T., Zou, L., Zhang, W., & Zhang, L. (2018). Extreme high-temperature events over East Asia in 1.5°C and 2°C warmer futures: Analysis of NCAR CESM low-warming experiments. *Geophysical Research Letters*, *45*(3), 1541–1550. https://doi.org/10.1002/2017gl076753

Li, L., Yu, Y., Tang, Y., Lin, P., Xie, J., Song, M., et al. (2020). The flexible global ocean-atmosphere-land system model grid-point version 3 (FGOALS-g3): Description and evaluation. *Journal of Advances in Modeling Earth Systems*, *12*(9), 1–28. https://doi.org/10.1029/2019ms002012

Liao, W., Liu, X., Li, D., Luo, M., Wang, D., Wang, S., et al. (2018). Stronger contributions of urbanization to heat wave trends in wet climates. *Geophysical Research Letters*, *45*(20), 310–317. https://doi.org/10.1029/2018gl079679

Liu, Y., Chen, J., Pan, T., Liu, Y., Zhang, Y., Ge, Q., et al. (2020). Global socioeconomic risk of precipitation extremes under climate change. *Earth's Future*, *8*(9), 1–15. https://doi.org/10.1029/2019ef001331

Luo, M., & Lau, N. C. (2017). Heat waves in southern China: Synoptic behavior, long-term change, and urbanization effects. *Journal of Climate*, *30*(2), 703–720. https://doi.org/10.1175/jcli-d-16-0269.1

Ma, F., & Yuan, X. (2021). Impact of climate and population changes on the increasing exposure to summertime compound hot extremes. *Science of the Total Environment*, *772*, 1–11. https://doi.org/10.1016/j.scitotenv.2021.145004

Massonnet, F., Ménégoz, M., Acosta, M., Yepes-Arbós, X., Exarchou, E., & Doblas-Reyes, F. J. (2020). Replicability of the EC-Earth3 Earth system model under a change in computing environment. *Geoscientific Model Development*, *13*(3), 1165–1178. https://doi.org/10.5194/gmd-13-1165-2020

Mauritsen, T., Bader, J., Becker, T., Behrens, J., Bittner, M., Brokopf, R., et al. (2019). Developments in the MPI-M Earth system model version 1.2 (MPI-ESM1.2) and its response to increasing CO_2. *Journal of Advances in Modeling Earth Systems*, *11*(4), 998–1038.

Mazdiyasni, O., AghaKouchak, A., Davis, S. J., Madadgar, S., Mehran, A., Ragno, E., et al. (2017). Increasing probability of mortality during Indian heat waves. *Science Advances*, *3*(6), 1–6. https://doi.org/10.1126/sciadv.1700066

Meehl, G. A., & Ebaldi, C. (2004). More intense, more frequent, and longer lasting heat waves in the 21st century. *Science*, *305*(5686), 994–997. https://doi.org/10.1126/science.1098704

Mishra, V., Ambika, A. K., Asoka, A., Aadhar, S., Buzan, J., Kumar, R., & Huber, M. (2020). Moist heat stress extremes in India enhanced by irrigation. *Nature Geoscience*, *13*(11), 722–728. https://doi.org/10.1038/s41561-020-00650-8

Mishra, V., Mukherjee, S., Kumar, R., & Stone, D. A. (2017). Heat wave exposure in India in current, 1.5°C, and 2°C worlds. *Environmental Research Letters*, *12*(12), 1–9. https://doi.org/10.1088/1748-9326/aa9388

Mondal, S. K., Huang, J., Wang, Y., Su, B., Zhai, J., Tao, H., et al. (2021). Doubling of the population exposed to drought over South Asia: CMIP6 multi-model-based analysis. *Science of the Total Environment*, *771*, 1–17. https://doi.org/10.1016/j.scitotenv.2021.145186

Mueller, V., Gray, C., & Kosec, K. (2014). Heat stress increases long-term human migration in rural Pakistan. *Nature Climate Change*, *4*(12), 182–185. https://doi.org/10.1038/nclimate2103

Mukherjee, S., & Mishra, V. (2018). A sixfold rise in concurrent day and night-time heatwaves in India under 2°C warming. *Scientific Reports*, *8*(1), 1–10. https://doi.org/10.1038/s41598-018-35348-w

Murakami, D., & Yamagata, Y. (2019). Estimation of gridded population and GDP scenarios with spatially explicit statistical downscaling. *Sustainability (Switzerland)*, *11*(7), 1–18. https://doi.org/10.3390/su11072106

Nasim, W., Amin, A., Fahad, S., Awais, M., Khan, N., Mubeen, M., et al. (2018). Future risk assessment by estimating historical heat wave trends with projected heat accumulation using SimCLIM climate model in Pakistan. *Atmospheric Research*, *205*(2), 118–133. https://doi.org/10.1016/j.atmosres.2018.01.009

O'Neill, B. C., Tebaldi, C., Van Vuuren, D. P., Eyring, V., Friedlingstein, P., Hurtt, G., et al. (2016). The scenario model intercomparison project (ScenarioMIP) for CMIP6. *Geoscientific Model Development*, *9*(9), 3461–3482.

Panda, D. K., AghaKouchak, A., & Ambast, S. K. (2017). Increasing heat waves and warm spells in India, observed from a multiaspect framework. *Journal of Geophysical Research: Atmospheres*, *122*(7), 3837–3858. https://doi.org/10.1002/2016jd026292

Pathak, A., Ghosh, S., Kumar, P., & Murtugudde, R. (2017). Role of oceanic and terrestrial atmospheric moisture sources in intraseasonal variability of Indian summer monsoon rainfall. *Scientific Reports*, *7*(1), 1–11. https://doi.org/10.1038/s41598-017-13115-7

Pepin, N., Bradley, R. S., Diaz, H. F., Baraer, M., Caceres, E. B., Forsythe, N., et al. (2015). Elevation-dependent warming in mountain regions of the world. *Nature Climate Change*, *5*(5), 424–430.

Perkins, S. E., & Alexander, L. V. (2013). On the measurement of heat waves. *Journal of Climate*, *26*(7), 4500–4517. https://doi.org/10.1175/jcli-d-12-00383.1

Raei, E., Nikoo, M. R., Aghakouchak, A., Mazdiyasni, O., & Sadegh, M. (2018). GHWR, a multi-method global heatwave and warm-spell record and toolbox. *Scientific Data*, *5*(180206), 1–15.

Ramachandran, S., & Kedia, S. (2013). Aerosol optical properties over South Asia from ground-based observations and remote sensing: A review. *Climate*, *1*(3), 84–119. https://doi.org/10.3390/cli1030084

Riahi, K., Van Vuuren, D. P., Kriegler, E., Edmonds, J., O'Neill, B. C., Fujimori, S., et al. (2017). The shared socioeconomic pathways and their energy, land use, and greenhouse gas emissions implications: An overview. *Global Environmental Change*, *42*, 153–168. https://doi.org/10.1016/j.gloenvcha.2016.05.009

Rohat, G., Flacke, J., Dosio, A., Dao, H., & Van Maarseveen, M. (2019). Projections of human exposure to dangerous heat in african cities under multiple socioeconomic and climate scenarios. *Earth's Future*, *7*(5), 528–546. https://doi.org/10.1029/2018ef001020

Rohini, P., Rajeevan, M., & Mukhopadhay, P. (2019). Future projections of heat waves over India from CMIP5 models. *Climate Dynamics*, *53*(1), 975–988. https://doi.org/10.1007/s00382-019-04700-9

Rohini, P., Rajeevan, M., & Srivastava, A. K. (2016). On the variability and increasing trends of heat waves over India. *Scientific Reports*, *6*(10), 1–9. https://doi.org/10.1038/srep26153

Russo, S., Sillmann, J., Sippel, S., Barcikowska, M. J., Ghisetti, C., Smid, M., & O'Neill, B. (2019). Half a degree and rapid socioeconomic development matter for heatwave risk. *Nature Communications*, *10*(1), 1–9. https://doi.org/10.1038/s41467-018-08070-4

Russo, S., Sillmann, J., & Sterl, A. (2017). Humid heat waves at different warming levels. *Scientific Reports*, *7477*(7), 1–7. https://doi.org/10.1038/s41598-017-07536-7

Saeed, F., Almazroui, M., Islam, N., & Khan, M. S. (2017). Intensification of future heat waves in Pakistan: A study using CORDEX regional climate models ensemble. *Natural Hazards*, *87*(3), 1635–1647. https://doi.org/10.1007/s11069-017-2837-z

Scovronick, N., Sera, F., Schneider, R., Tobias, A., Astrom, C., Guo, Y., et al. (2018). The burden of heat-related mortality attributable to recent human-induced climate change. *Nature Climate Change*, 1–18.

Seland, Ø., Bentsen, M., Seland Graff, L., Olivié, D., Toniazzo, T., Gjermundsen, A., et al. (2020). The Norwegian Earth system model, NorESM2 – evaluation of theCMIP6 DECK and historical simulations. *Geoscientific Model Development Discussions*, *13*, 6165–6200. https://doi.org/10.5194/gmd-13-6165-2020

Semmler, T., Danilov, S., Gierz, P., Goessling, H. F., Hegewald, J., Hinrichs, C., et al. (2020). Simulations for CMIP6 with the AWI climate model AWI-CM-1-1. *Journal of Advances in Modeling Earth Systems*, *12*(9), 1–34. https://doi.org/10.1029/2019ms002009

Sen, A., Abdelmaksoud, A. S. S., Nazeer Ahammed, Y., Alghamdi, M. A., Banerjee, T., Bhat, M. A., et al. (2017). Variations in particulate matter over Indo-Gangetic plains and Indo-Himalayan range during four field campaigns in winter monsoon and summer monsoon: Role of pollution pathways. *Atmospheric Environment*, *154*, 200–224. https://doi.org/10.1016/j.atmosenv.2016.12.054

Shen, L., Zhang, Y., Ullah, S., Pepin, N., & Ma, Q. (2021). Changes in snow depth under elevation-dependent warming over the tibetan plateau. *Atmospheric Science Letters*, *22*(5), 1–12. https://doi.org/10.1002/asl.1041

Shi, X., Chen, J., Gu, L., Xu, C. Y., Chen, H., & Zhang, L. (2021). Impacts and socioeconomic exposures of global extreme precipitation events in 1.5 and 2.0°C warmer climates. *Science of the Total Environment*, *760*(1–13), 142665. https://doi.org/10.1016/j.scitotenv.2020.142665

Shi, Z., Xu, X., & Jia, G. (2021). Urbanization magnified nighttime heat waves in China. *Geophysical Research Letters*, *48*(15), 1–11. https://doi.org/10.1029/2021gl093603

Smirnov, O., Zhang, M., Xiao, T., Orbell, J., Lobben, A., & Gordon, J. (2016). The relative importance of climate change and population growth for exposure to future extreme droughts. *Climatic Change*, *138*(1–2), 41–53. https://doi.org/10.1007/s10584-016-1716-z

Sun, C., Jiang, Z., Li, W., Hou, Q., & Li, L. (2019). Changes in extreme temperature over China when global warming stabilized at 1.5°C and 2.0°C. *Scientific Reports*, *9*(1), 1–11. https://doi.org/10.1038/s41598-019-50036-z

Sun, H., Wang, Y., Chen, J., Zhai, J., Jing, C., Zeng, X., et al. (2017). Exposure of population to droughts in the Haihe River Basin under global warming of 1.5 and 2.0°C scenarios. *Quaternary International*, *453*, 74–84. https://doi.org/10.1016/j.quaint.2017.05.005

Swart, N. C., Cole, J. N. S., Kharin, V. V., Lazare, M., Scinocca, J. F., Gillett, N. P., et al. (2019). The Canadian earth system model version 5 (CanESM5.0.3). *Geoscientific Model Development*, *12*(11), 4823–4873. https://doi.org/10.5194/gmd-12-4823-2019

Tatebe, H., Ogura, T., Nitta, T., Komuro, Y., Ogochi, K., Takemura, T., et al. (2018). Description and basic evaluation of simulated mean state, internal variability, and climate sensitivity in MIROC6. *Geoscientific Model Development Discussions*, *12*, 2727–2765.

Trenberth, E. K., Fasullo, T., Sheperd, J., & Theodore, G. (2015). Attribution of climate extreme events. *Nature Climate Change*, *5*(1), 725–730. https://doi.org/10.1038/nclimate2657

Ullah, S., You, Q., Ullah, W., Hagan, D. F. T., Ali, A., Ali, G., et al. (2019). Daytime and night-time heat wave characteristics based on multiple indices over the China–Pakistan economic corridor. *Climate Dynamics*, *53*(9–10), 6329–6349. https://doi.org/10.1007/s00382-019-04934-7

Ullah, S., You, Q., Zhang, Y., Bhatti, A. S., Ullah, W., Hagan, D. F. T., et al. (2020). Evaluation of CMIP5 models and projected changes in temperatures over South Asia under global warming of 1.5°C, 2°C and 3°C. *Atmospheric Research*, *246*, 1–18. https://doi.org/10.1016/j.atmosres.2020.105122

Viviroli, D., Kummu, M., Meybeck, M., Kallio, M., & Wada, Y. (2020). Increasing dependence of lowland populations on mountain water resources. *Nature Sustainability*, *3*(11), 917–928. https://doi.org/10.1038/s41893-020-0559-9

Vogel, M. M., Zscheischler, J., Wartenburger, R., Dee, D., & Seneviratne, S. I. (2019). Concurrent 2018 hot extremes across northern hemisphere due to human-induced climate change. *Earth's Future*, *7*(7), 692–703. https://doi.org/10.1029/2019ef001189

Volodin, E. M., Mortikov, E. V., Kostrykin, S. V., Galin, V. Y., Lykossov, V. N., Gritsun, A. S., et al. (2017). Simulation of the present-day climate with the climate model INMCM5. *Climate Dynamics*, *49*(11–12), 3715–3734. https://doi.org/10.1007/s00382-017-3539-7

Volodin, E. M., Mortikov, E. V., Kostrykin, S. V., Galin, V. Y., Lykossov, V. N., Gritsun, A. S., et al. (2018). Simulation of the modern climate using the INM-CM48 climate model. *Russian Journal of Numerical Analysis and Mathematical Modelling*, *33*(6), 367–374. https://doi.org/10.1515/rnam-2018-0032

Wang, A., Wang, Y., Su, B., Kundzewicz, Z. W., Tao, H., Wen, S., et al. (2020). Comparison of changing population exposure to droughts in river basins of the tarim and the Indus. *Earth's Future*, *8*(5), 1–13. https://doi.org/10.1029/2019ef001448

Wang, J., Chen, Y., Tett, S. F. B., Yan, Z., Zhai, P., Feng, J., & Xia, J. (2020). Anthropogenically-driven increases in the risks of summertime compound hot extremes. *Nature Communications*, *11*(1), 1–11. https://doi.org/10.1038/s41467-019-14233-8

Wang, Y., Wang, A., Zhai, J., Tao, H., Jiang, T., Su, B., et al. (2019). Tens of thousands additional deaths annually in cities of China between 1.5°C and 2.0°C warming. *Nature Communications*, *10*(1), 1–7. https://doi.org/10.1038/s41467-019-11283-w

Watts, N., Amann, M., Arnell, N., Ayeb-Karlsson, S., Beagley, J., Belesova, K., et al. (2021). The 2020 report of the lancet countdown on health and climate change: Responding to converging crises. *The Lancet*, *397*(10269), 129–170. https://doi.org/10.1016/s0140-6736(20)32290-x

Watts, N., Amann, M., Arnell, N., Ayeb-Karlsson, S., Belesova, K., Boykoff, M., et al. (2019). The 2019 report of the lancet countdown on health and climate change: Ensuring that the health of a child born today is not defined by a changing climate. *The Lancet*, *394*(10211), 1836–1878. https://doi.org/10.1016/s0140-6736(19)32596-6

Wen, S., Wang, A., Tao, H., Malik, K., Huang, J., Zhai, J., et al. (2019). Population exposed to drought under the 1.5°C and 2.0°C warming in the Indus river basin. *Atmospheric Research*, *218*, 296–305. https://doi.org/10.1016/j.atmosres.2018.12.003

Wu, T., Lu, Y., Fang, Y., Xin, X., Li, L., Li, W., et al. (2019). The Beijing climate center climate system model (BCC-CSM): The main progress from CMIP5 to CMIP6. *Geoscientific Model Development*, *12*(4), 1573–1600. https://doi.org/10.5194/gmd-12-1573-2019

Wyser, K., Van Noije, T., Yang, S., Von Hardenberg, J., O'Donnell, D., & Döscher, R. (2020). On the increased climate sensitivity in the EC-Earth model from CMIP5 to CMIP6. *Geoscientific Model Development*, *13*(8), 3465–3474. https://doi.org/10.5194/gmd-13-3465-2020

Xie, W., Zhou, B., You, Q., Zhang, Y., & Ullah, S. (2020). Observed changes in heat waves with different severities in China during 1961–2015. *Theoretical and Applied Climatology*, *141*(3–4), 1529–1540. https://doi.org/10.1007/s00704-020-03285-2

Xu, Y., Wu, X., Kumar, R., Barth, M., Diao, C., Gao, M., et al. (2020). Substantial increase in the joint occurrence and human exposure of heatwave and high-PM hazards over South Asia in the mid-21st century. *AGU Advances*, *1*(2), 1–19. https://doi.org/10.1029/2019av000103

You, Q., Chen, D., Wu, F., Pepin, N., Cai, Z., Ahrens, B., et al. (2020). Elevation dependent warming over the tibetan plateau: Patterns, mechanisms and perspectives. *Earth-Science Reviews*, *210*, 1–19. https://doi.org/10.1016/j.earscirev.2020.103349

You, Q., Jiang, Z., Kong, L., Wu, Z., Bao, Y., Kang, S., & Pepin, N. (2017). A comparison of heat wave climatologies and trends in China based on multiple definitions. *Climate Dynamics*, *48*(11–12), 3975–3989. https://doi.org/10.1007/s00382-016-3315-0

You, Q., Ren, G., Zhang, Y., Ren, Y., Sun, X., Zhan, Y., et al. (2017). An overview of studies of observed climate change in the Hindu Kush Himalayan (HKH) region. *Advances in Climate Change Research*, *8*(3), 141–147. https://doi.org/10.1016/j.accre.2017.04.001

Yukimoto, S., Kawai, H., Koshiro, T., Oshima, N., Yoshida, K., Urakawa, S., et al. (2019). The meteorological research institute earth system model version 2.0, MRI-ESM2.0: Description and basic evaluation of the physical component. *Journal of the Meteorological Society of Japan*, *97*(5), 931–965. https://doi.org/10.2151/jmsj.2019-051

Zhai, J., Mondal, S. K., Fischer, T., Wang, Y., Su, B., Huang, J., et al. (2020). Future drought characteristics through a multi-model ensemble from CMIP6 over South Asia. *Atmospheric Research*, *246*, 1–18. https://doi.org/10.1016/j.atmosres.2020.105111

Zhan, M., Li, X., Sun, H., Zhai, J., Jiang, T., & Wang, Y. (2018). Changes in extreme maximum temperature events and population exposure in China under global warming scenarios of 1.5 and 2.0°C: Analysis using the regional climate model COSMO-CLM. *Journal of Meteorological Research*, *32*(1), 99–112. https://doi.org/10.1007/s13351-018-7016-y

Zhang, W., Zhou, T., Zou, L., Zhang, L., & Chen, X. (2018). Reduced exposure to extreme precipitation from 0.5°C less warming in global land monsoon regions. *Nature Communications*, *9*(1), 1–8. https://doi.org/10.1038/s41467-018-05633-3

Zhang, Y., Mao, G., Chen, C., Lu, Z., Luo, Z., & Zhou, W. (2020). Population exposure to concurrent daytime and nighttime heatwaves in Huai River Basin, China. *Sustainable Cities and Society*, *61*, 1–16. https://doi.org/10.1016/j.scs.2020.102309

Zhao, J. T., Su, B. D., Mondal, S. K., Wang, Y. J., Tao, H., & Jiang, T. (2021). Population exposure to precipitation extremes in the Indus River Basin at 1.5°C, 2.0°C and 3.0°C warming levels. *Advances in Climate Change Research*, *12*, 199–209. https://doi.org/10.1016/j.accre.2021.03.005

Zscheischler, J., Westra, S., Van Den Hurk, B. J. J. M., Seneviratne, S. I., Ward, P. J., Pitman, A., et al. (2018). Future climate risk from compound events. *Nature Climate Change*, *8*(6), 469–477. https://doi.org/10.1038/s41558-018-0156-3